

# Classical helicity of superfluid helium

C. F. Barenghi<sup>1,\*</sup>, L. Galantucci<sup>1</sup>, N.G. Parker<sup>1</sup>, and A. W. Baggaley<sup>1</sup>

<sup>1</sup>Joint Quantum Centre Durham-Newcastle (JQC), School of Mathematics, Statistics and Physics Newcastle University, Newcastle upon Tyne NE1 7RU, UK

\*carlo.barenghi@newcastle.ac.uk

## ABSTRACT

Helicity - a quadratic invariant of the classical Euler equation like the energy - plays a fundamental role in turbulent flows, controlling the strength of the nonlinear interactions which cascade energy to smaller length scales. The growing interest in turbulent superfluid liquid helium, a disordered state of quantum matter consisting of a tangle of vortex lines - triggers a natural question: what is superfluid helicity? The most used model of superfluid vortex lines is based on the Gross-Pitaevskii equation for a weakly interacting Bose gas. In this mean field model, unfortunately, helicity is ill-defined, as vorticity and velocity are singular on the centerline of the vortex. Here we show that by taking into account more realistic features of the vortex core arising from N-body quantum mechanics simulations, which account for the stronger atom interactions occurring in a liquid, the classical definition of helicity can be extended to superfluid helium. We also present results of numerical experiments which reveal the role and physical meaning of helicity in superfluid turbulence.

## 1 Introduction

### Why helicity?

The success in creating knotted vortices under controlled laboratory conditions<sup>1</sup> has stimulated a great interest in quantifying the amount of linkage of vortex lines in turbulent flows. The quantity which is ideally suited for this task is the helicity<sup>2</sup>, defined as

$$H(t) = \int_V \boldsymbol{\omega}(\mathbf{r}, t) \cdot \mathbf{v}(\mathbf{r}, t) d^3\mathbf{r}, \quad (1)$$

where  $\mathbf{v} = \mathbf{v}(\mathbf{r}, t)$  is the velocity field,  $\boldsymbol{\omega} = \boldsymbol{\omega}(\mathbf{r}, t) = \nabla \times \mathbf{v}$  is the vorticity,  $\mathbf{r}$  is the position,  $t$  is time, and  $V$  is the volume of the region which contains the fluid. In the absence of viscous forces, the flow  $\mathbf{v}$  evolves according to the Euler equation, conserving, in addition to energy, also helicity, being the topology frozen as a result of Kelvin's circulation theorem. If the vorticity is concentrated in thin tubes carrying the same vorticity flux (circulation)  $\kappa$ , helicity can be expressed as<sup>3</sup>

$$H(t) = \kappa^2 [Wr(t) + Lk(t) + Tw(t)], \quad (2)$$

where  $Wr$ ,  $Lk$  and  $Tw$  are respectively the amount of writhing, linking and twisting of the vortex tubes. The physical importance of helicity cannot be understated. For example, a large helicity weakens the nonlinearity of the Navier-Stokes equation in turbulent flows, reducing the direct cascade of energy from large to small length scales<sup>4</sup>; at the same time, the interaction of helical modes of the same sign favours the three-dimensional inverse energy transfer<sup>5</sup>; in astrophysics, helicity quantifies the lack of mirror symmetry of the flow which favours the generation of magnetic field by dynamo action<sup>6</sup>. The possibility of a vortex knot cascade<sup>7,8</sup> in the decay of turbulence, and new experimental techniques to measure directly the helicity of thin-cored vortices<sup>9</sup> add to the physical interest.

Superfluid liquid helium<sup>10</sup> is an ideal context to investigate the linkage of turbulent vortex lines for two reasons. Firstly, unlike ordinary (classical) flows whose vorticity is a continuous field and where the vortex-core size is arbitrary, superfluid vorticity is concentrated in vortex line filaments of fixed thickness ( $a_0 \approx 10^{-10}$  m) and fixed quantized circulation  $\kappa = h/m \approx 10^{-7}$  m<sup>2</sup>/s, where  $h$  is Planck's constant and  $m$  is the mass of a helium atom. Secondly, at sufficiently low temperatures, thermal excitations are negligible and helium is effectively a pure inviscid superfluid, making the classical Euler equation particularly relevant, even though it is worth underlining that there is no constraint on helicity conservation as topology is not frozen (*i.e.* vortex reconnections can occur). A state of superfluid turbulence<sup>11,12</sup> is easily generated in liquid helium by thermal or mechanical stirring, and takes the form of a tangle of vortex lines. New flow visualization techniques<sup>13,14</sup> suitable for temperatures near absolute zero have led to significant progress in understanding the dynamics of tangled vortex lines.

It has been found that, in some flow regimes and at some length scales, superfluid turbulence shares important properties with ordinary turbulence<sup>15,16</sup>; in other regimes, superfluid turbulence appears quite different<sup>17</sup>. Finally, it is now possible to experimentally observe individual vortex reconnections events, both in superfluid helium<sup>18</sup> and in related gaseous atomic Bose-Einstein condensates<sup>19</sup>.

It is therefore natural to ask if helicity is a useful concept in the superfluid context. But what is the definition of superfluid helicity? What is its role in superfluid turbulence? In this letter we address these important questions.

### The GPE model of the superfluid vortex core

A microscopic mean field model of superfluids which is often used in the literature is the Gross-Pitaevskii equation (GPE)<sup>10</sup> for the complex wavefunction  $\psi = \psi(\mathbf{r}, t)$  of a weakly-interacting dilute Bose-Einstein condensate. By writing  $\psi$  in terms of its amplitude and phase,  $\psi(\mathbf{r}, t) = \sqrt{n(\mathbf{r}, t)}e^{i\phi(\mathbf{r}, t)}$ , the condensate can be interpreted as a fluid with mass density  $n(\mathbf{r}, t)m$  and velocity  $\mathbf{v}(\mathbf{r}, t) = (\hbar/m)\nabla\phi(\mathbf{r}, t)$ . It can be shown<sup>10</sup> that this fluid obeys the continuity equation and the Euler equation - the latter containing an additional ‘quantum pressure’ term, responsible for vortex reconnections. Furthermore, at distances larger than the healing length  $\hbar/\sqrt{nmg}$  (where  $g$  is a constant proportional to the scattering length of helium atoms), the quantum pressure becomes negligible, recovering the classical Euler equation for a compressible barotropic fluid of pressure  $p = gn^2/2$ .

In the GPE model, vortex lines are phase singularities: a vortex is a tubular hole along a curve  $\mathbf{r}_0 = \mathbf{r}_0(\xi)$  (where  $\xi$  is the arclength) at which  $\psi = 0$  exactly. The change of the phase along an arbitrary closed contour around the centerline of the vortex is  $2\pi$ , corresponding to circulation  $\kappa$ . The changing phase implies an azimuthal vortex flow around the centerline,  $v_\theta = \kappa/(2\pi r)$  (where  $r$  is the radial distance). Quantum mechanics constrains not only the circulation but also the size of the hole: the superfluid density  $n(\mathbf{r}, t)$  drops from its bulk value (away from the vortex) to zero (at the centerline) over a distance (called the vortex core radius  $a_0$ ) which is of the order of magnitude of the healing length.

In summary, according to the GPE model of the vortex, the superfluid velocity is irrotational everywhere (including the core region) with the exception of the vortex centerline (where  $v_\theta \rightarrow \infty$  but  $n \rightarrow 0$ , keeping the momentum finite). The vorticity can thus be interpreted as a Dirac delta function (a distribution) centered on the centerline. The problem with this model of the vortex core is that the standard definition of helicity, Eq. (1), becomes ill-behaved as both velocity and vorticity are singular on the centerline (in the direction perpendicular to it). Being the vorticity a distribution, if we attempt to define helicity by integrating  $\boldsymbol{\omega}$  against a test function, we find that  $\mathbf{v}$  is not a suitably smooth test function. The second definition of helicity, Eq. (2), has a problem too: the twist  $Tw$  consists of two contributions: normalized torsion and intrinsic twist; the latter requires the introduction of a ribbon, or a second vortex line along the centerline under consideration. However, a GPE vortex contains only *one* vortex line within the core - the centerline itself - and the core lacks any internal structure to define an intrinsic twist. These difficulties are discussed in the current literature<sup>20–23</sup> where ingenious solutions and possible definitions of superfluid helicity are proposed.

### A more physical model of the superfluid vortex core

Although the GPE mean field model describes the dynamics of atomic Bose-Einstein condensates to a very high degree of accuracy (provided their temperature is significantly lower than the critical temperature), it is a poor model of superfluid <sup>4</sup>He (which is a liquid, not a dilute gas of weakly interacting atoms). Indeed it has been known for a some time<sup>10</sup> that the energy spectrum  $E(k)$  of the elementary excitations of the uniform solution of the GPE consists of phonons at small wavenumber  $k$  and free particles at large  $k$ , without the maxon peak and the roton dip which are characteristic of liquid helium<sup>24</sup>. Maxons and rotons require a more sophisticated many-body quantum mechanical description, which determines the true nature of the vortex core<sup>25</sup>. This description, as we summarize below, shows that the helium vortex structure is more complex<sup>26</sup> than predicted by the GPE.

Consider a straight helium vortex. The  $N$ -body wavefunction  $\Psi(\mathbf{R})$  where  $\mathbf{R} = (\mathbf{r}_1, \mathbf{r}_2, \dots, \mathbf{r}_N)$  contains the coordinates of  $N$  atoms, must be an eigenstate of the angular momentum operator with eigenvalues which are integer multiples of  $N\hbar$ . Therefore  $\Psi(\mathbf{R})$  must be complex,  $\Psi(\mathbf{R}) = \Psi_0(\mathbf{R})e^{i\Omega(\mathbf{R})}$ , where  $\Omega(\mathbf{R})$  is the phase. The standard approach (fixed phase approximation) consists in choosing  $\Omega(\mathbf{R})$  and solving the resulting Schroedinger equation for  $\Psi_0(\mathbf{R})$  allowing interatomic correlations at short distances. The simplest choice for the phase is the Onsager-Feynman phase  $\Omega(\mathbf{R}) = \sum_{j=1}^N \theta_j$  where  $\theta_j$  is the azimuthal angle of atom  $j$  with respect to the centerline of the vortex. This choice gives rise to a velocity field which is irrotational everywhere but on the centerline, where it diverges, making the vorticity a Dirac delta function localized on the centerline, as in the GPE model. The equation for  $\Psi_0(\mathbf{R})$  yields a density profile  $n$  which vanishes at the centerline (as in the GPE model), but which also displays density oscillations near the edge of the core; these oscillations have wavenumbers typical of rotons (the density oscillations and the maxon-roton feature of the energy spectrum are also captured by the nonlocal GPE<sup>27</sup>).

This vortex model can be improved (yielding lower vortex energy, in better agreement with experiments) if the Onsager-Feynman assumption is taken only as initial guess and inter-particle correlations are taken into account also in determining

the phase<sup>28</sup>. The improved model yields features<sup>28,29</sup> which are important for helicity and are schematically summarized in Fig. 1: the density drops in the core (as for the GPE model) but remains nonzero on the centerline, and the azimuthal velocity acquires the form of a Rankine vortex, with crossover from  $v_\theta \sim r$  behaviour to  $v_\theta \sim 1/r$  behaviour at  $r \approx a_0$ : this second feature means that the vorticity is approximately constant inside the core.

## 2 Helicity for non singular superfluid vortices

Since vorticity and velocity are finite and well-behaved in the core region, including the centerline itself, there is no conceptual difficulty in applying the classical definition of helicity, Eq. (1), to superfluid helium. The right hand side of Eq. (1) can be evaluated using the result that the vorticity  $\boldsymbol{\omega}$  is zero everywhere but in narrow tubes of constant cross sectional area  $\pi a_0^2$  along the vortex lines, where it has constant magnitude  $\omega = \kappa/(\pi a_0^2)$  and its direction is tangential to the vortex centerline. It is therefore possible to reduce the volume integral in Eq. (1) as it follows (to simplify the notation we have omitted the time dependence):

$$H = \sum_{i=1}^N \oint_{\mathcal{T}_i} \boldsymbol{\omega}(\mathbf{r}) \cdot \mathbf{v}(\mathbf{r}) d^3\mathbf{r} = \sum_{i=1}^N \int_0^{L_i} d\xi \int_{\mathcal{D}_\xi} d^2\boldsymbol{\sigma} \boldsymbol{\omega}(\xi, \boldsymbol{\sigma}) \cdot \mathbf{v}(\xi, \boldsymbol{\sigma}) = \frac{\kappa}{\pi a_0^2} \sum_{i=1}^N \int_0^{L_i} d\xi \int_{\mathcal{D}_\xi} d^2\boldsymbol{\sigma} \mathbf{s}'(\xi) \cdot \mathbf{v}(\xi, \boldsymbol{\sigma}) , \quad (3)$$

where  $N$  is the number of superfluid vortex lines present in the flow;  $\mathbf{s}(\xi)$  is the position of a generic point along the vortex line parametrized by the arc length  $\xi$ ;  $\mathbf{s}'(\xi) = d\mathbf{s}(\xi)/d\xi$  is the unit tangent vector to the vortex line at  $\mathbf{s}(\xi)$ ;  $\mathcal{T}_i$  is the tube of circular cross sectional area  $\pi a_0^2$  centred on the  $i$ -th vortex line of length  $L_i$ ;  $\mathcal{D}_\xi$  is the disc of radius  $a_0$ , centred in  $\mathbf{s}(\xi)$  and perpendicular to  $\mathbf{s}'(\xi)$ ;  $\boldsymbol{\sigma} = \boldsymbol{\sigma}(r, \theta)$  is the position vector on the disc  $\mathcal{D}_\xi$  and depends on the distance  $r$  from its centre  $\mathbf{s}(\xi)$  and the azimuthal angle  $\theta$  (see Supplementary Material, Fig. 3).

The superfluid velocity  $\mathbf{v}(\xi, \boldsymbol{\sigma})$  arises from three different contributions: (i) any (irrotational) superflow  $\mathbf{v}_{ext}(\xi, \boldsymbol{\sigma})$  imposed externally (for example, by a heater or by bellows); (ii) the velocity field  $\mathbf{v}_i(\xi, \boldsymbol{\sigma})$  induced, (via the Biot-Savart law) by all line elements of the  $i$ -th vortex line; (iii) the velocity  $\mathbf{v}_{j \neq i}(\xi, \boldsymbol{\sigma}) = \sum_{j \neq i} \mathbf{v}_j(\xi, \boldsymbol{\sigma})$  induced (via the Biot-Savart law) by all the other vortex lines. In superfluid helium (in contrast to *e.g.* atomic Bose-Einstein condensates), the core size  $a_0 \simeq 10^{-10}$  m is much smaller than both the large scale of the system,  $D$ , and the average inter-vortex spacing,  $\ell$ . Typical experimental values are  $D/a_0 \sim 10^7 \div 10^8$  and  $\ell/a_0 \sim 10^4 \div 10^6$ . As a consequence, both the external superflow  $\mathbf{v}_{ext}$  and the superfluid velocity field induced by all the other vortices  $\mathbf{v}_{j \neq i}$  are constant on the disc  $\mathcal{D}_\xi$  and can be evaluated at  $\mathbf{s}(\xi)$ , *i.e.*  $\mathbf{v}_{ext}(\xi, \boldsymbol{\sigma}) = \mathbf{v}_{ext}(\mathbf{s}(\xi))$  and  $\mathbf{v}_{j \neq i}(\xi, \boldsymbol{\sigma}) = \mathbf{v}_{j \neq i}(\mathbf{s}(\xi))$ .

In addition, the atomic size of the vortex core also implies that typical values of the radius of curvature  $R_c$  are much larger than the vortex core itself,  $R_c \sim 10^5 a_0$ . The neighbourhood  $|\xi - \xi'| < \delta$  of the vortex line near the generic point  $\mathbf{s}(\xi)$  appears hence effectively straight and perpendicular to the disc  $\mathcal{D}_\xi$  at distances  $a_0 \ll \delta \ll R_c$  where  $R_c = 1/|d^2\mathbf{s}/d\xi^2|$  is the local radius of curvature at  $\mathbf{s}(\xi)$ ; therefore at such distances, the superfluid velocity field  $\mathbf{v}_i^{near}(\xi, \boldsymbol{\sigma})$  induced by the closest vortex line elements on  $\mathcal{D}_\xi$  is perpendicular to the unit tangent vector  $\mathbf{s}'(\xi)$ , yielding zero contribution to the helicity (*cfr.* Eq. (3)). As a consequence, the only non zero contribution of the  $i$ -th vortex line to helicity arises from the line elements sufficiently distant from  $\mathcal{D}_\xi$ , where the induced velocity  $\mathbf{v}_i^{far}(\xi, \boldsymbol{\sigma})$  is constant and can be evaluated at  $\mathbf{s}(\xi)$ , *i.e.*  $\mathbf{v}_i^{far}(\xi, \boldsymbol{\sigma}) = \mathbf{v}_i^{far}(\mathbf{s}(\xi))$ . Eq. 3 thus becomes

$$\begin{aligned} H &= \frac{\kappa}{\pi a_0^2} \sum_{i=1}^N \int_0^{L_i} d\xi \int_{\mathcal{D}_\xi} d^2\boldsymbol{\sigma} \mathbf{s}'(\xi) \cdot \left[ \mathbf{v}_{ext}(\mathbf{s}(\xi)) + \mathbf{v}_i^{near}(\xi, \boldsymbol{\sigma}) + \mathbf{v}_i^{far}(\mathbf{s}(\xi)) + \mathbf{v}_{j \neq i}(\mathbf{s}(\xi)) \right] \\ &= \kappa \sum_{i=1}^N \int_0^{L_i} d\xi \mathbf{s}'(\xi) \cdot \mathbf{v}_{nl}(\mathbf{s}(\xi)) , \end{aligned} \quad (4)$$

where  $\mathbf{v}_{nl}(\mathbf{s}(\xi)) = \mathbf{v}_{ext}(\mathbf{s}(\xi)) + \mathbf{v}_i^{far}(\mathbf{s}(\xi)) + \mathbf{v}_{j \neq i}(\mathbf{s}(\xi))$  is the *non-local* superfluid velocity at  $\mathbf{s}(\xi)$ , *i.e.* the superfluid velocity field induced by distant vortex line elements. We conclude that superfluid helicity measures the non-local contribution<sup>30</sup> to the superfluid velocity; geometrically, superfluid helicity measures the non-local velocity's orientation with respect to the local polarization of the vortex lines. Helicity therefore accounts for the existence of coherent superfluid vorticity structures generating a large scale (non-local) flow, and the vortex tangle's topology.

What is the physical interpretation of this definition of helicity? We expect that, if the turbulent vortex lines are randomly oriented with respect to each other, the average magnitude of  $\mathbf{v}_{nl}$  will be zero (as velocity contributions at each point  $\mathbf{s}(\xi)$  on the vortex lines will tend to cancel each other out), and the helicity will be approximately zero. Viceversa, we expect that, if the vortex tangle is organized in bundles of quasi-parallel, highly polarized vortex lines responsible for the existence of

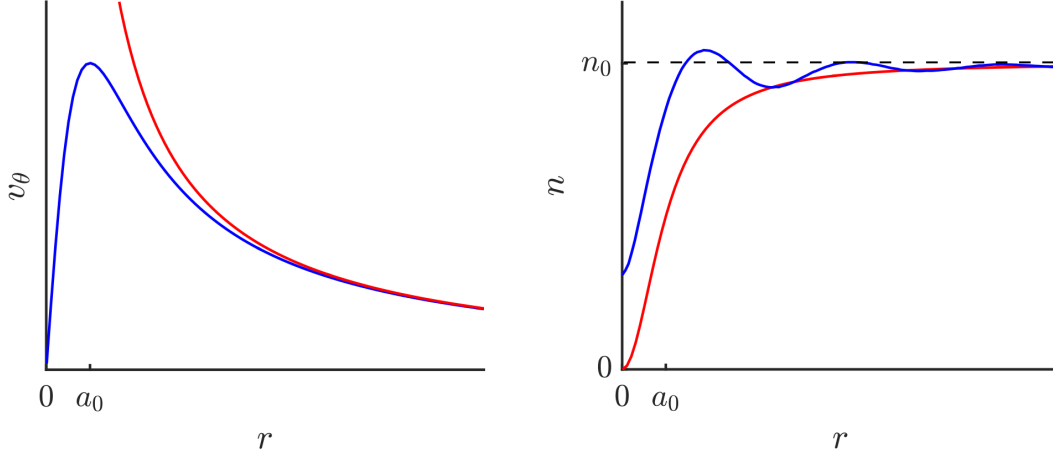


**Figure 1.** Schematic density profile  $n(r)$  vs  $r$  (right) and azimuthal velocity profile  $v_\theta$  vs  $r$  (left) in the mean field GPE model (red curves) and N-body quantum mechanics (blue curves) [data reproduced from Fig. 3 of Galli *et al*<sup>26</sup>].

regions of strong vorticity, the helicity might be large, as a result of the interplay between the vortex bundles and the large scale flow which they contribute to generate. On the last point, it is worth noting, in fact, that the existence of large scale flows is not a sufficient condition for large helical flows (*e.g* two straight parallel vortex lines create a large scale superflow but the total helicity is zero). The numerical simulations which we present in the next section confirm these expectations.

### 3 Numerical simulations

#### Model

In classical ideal fluids, helicity is conserved by the governing equation of motion, the Euler equation. In the case of superfluid helium, however, having left the safe ground of the GPE, we face the difficulty that there is no known hydrodynamical equation which describes the details of the flow at length scales as small as  $a_0$ . Information about the vortex core is limited, and comes from measurements of energy and velocity of vortex rings<sup>31</sup>, and from N-body quantum mechanics calculations for a static straight vortex.

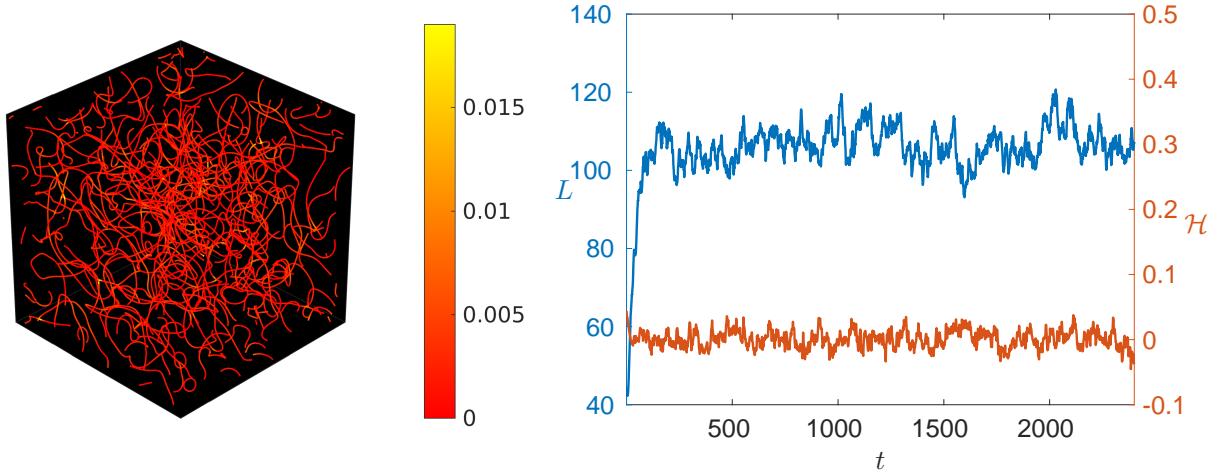
In order to demonstrate the physical interpretation of superfluid helicity which we have proposed, we perform a numerical experiment employing a *mesoscopic* description of superfluid helium dynamics: the Vortex Filament Model (VFM)<sup>32</sup>. The VFM, justified by the large  $\ell/a_0$  ratio ( $\approx 10^4 \div 10^6$ ), is an established and popular semi-classical approximation<sup>33</sup> in which vortex lines are represented as space curves  $\mathbf{s} = \mathbf{s}(\xi, t)$  of infinitesimal thickness which move according to Schwarz's equation (see Methods). The VFM accounts for the local balance between the Magnus force, arising from the local superfluid velocity and its circulation around the vortex core, and the temperature-dependent mutual friction force, dependent on the local relative velocity between the vortex line and the normal fluid. When two vortex lines collide they undergo a vortex reconnection, a phenomenon outside the realm of the Euler equation which has been observed in helium and Bose-Einstein condensates experiments<sup>18,19</sup> and in numerical simulations of the GPE<sup>34-37</sup>. In the VFM, reconnections are performed algorithmically<sup>32,38</sup>.

#### Results

Figure 2 shows snapshots of two different turbulent regimes computed using the VFM in periodic domains corresponding to approximately the same vortex line density (vortex length per unit volume)  $L \approx 100 \text{ cm}^{-2}$ . In both regimes, after an initial transient, a statistical steady-state of turbulence is achieved in which all the properties of turbulence fluctuate around well-defined mean values which are independent of the initial condition. The first turbulent regime is illustrated in Fig. 2(a); the figure shows a vortex tangle sustained by a uniform normal fluid, modelling a small applied heat flux in a large channel. The second regime is shown in Fig. 2(b): here the turbulence is driven by a normal fluid ABC flow<sup>39</sup>, modelling the coherent regions of high vorticity expected when an ordinary viscous fluid is turbulent.

In both panels of Fig. 2(left), the vortex lines are colour-coded according to the local absolute helicity density  $|\mathbf{s}'(\xi) \cdot \mathbf{v}_{nl}(\mathbf{s}(\xi))|$  as arising from Eq. (4). It is apparent that in Fig. 2(a) the helicity density is very small everywhere, whereas in Fig. 2(b) there are regions of strong helicity. This accounts for the difference between the two turbulent regimes observed in terms of the total helicity: the integrated values are  $H = 0 \pm 0.14 \text{ cm}^4/\text{s}^2$  for (a) and  $H = 2.91 \pm 0.04 \text{ cm}^4/\text{s}^2$  for (b). If we decompose the superfluid velocity at each point  $\mathbf{s}(\xi)$  along the vortex lines as  $\mathbf{v}(\mathbf{s}) = \mathbf{v}_i^{near}(\mathbf{s}(\xi)) + \mathbf{v}_{nl}(\mathbf{s}(\xi))$  (where  $\mathbf{v}_i^{near}(\mathbf{s}(\xi))$  is computed via the *local induction approximation*<sup>32</sup>, taking into account the small but non vanishing curvature

(a)



(b)

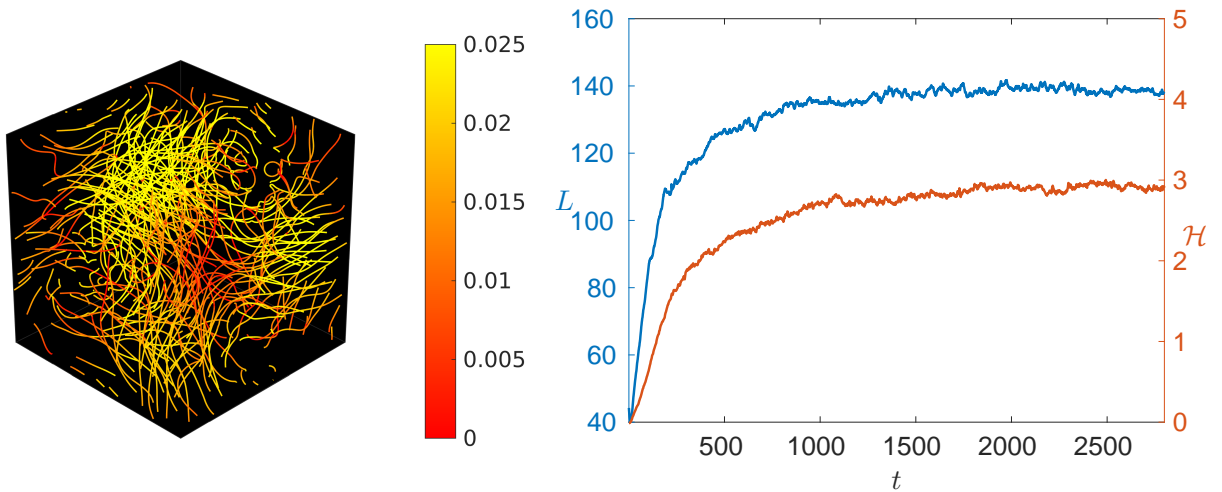


**Figure 2.** (Left) Snapshots of vortex tangles in two turbulence regimes with comparable vortex line density ( $L \approx 100 \text{ cm}^{-2}$ ) after the initial transient. In the first regime (a) the turbulence is driven by a uniform normal fluid, in the second regime by an ABC flow. The vortex line are colour-coded according to the local absolute helicity density value. (Right) Time series showing the evolution of the corresponding vortex line densities,  $L$  (in blue), and volume integrated helicity,  $H$  (in red).

of the vortex) and sample over the vortex configuration, we obtain  $\langle \mathbf{v}_{nl} \rangle / \langle \mathbf{v} \rangle \approx 0.29$  for (a) and  $\langle \mathbf{v}_{nl} \rangle / \langle \mathbf{v} \rangle \approx 2.4$  for (b): this qualitative, order-of-magnitude difference between the two turbulent regimes confirms the physical interpretation of helicity presented in the previous section.

The turbulence simulations which we have described include thousands of vortex reconnections. A natural question is what happens to helicity during a single vortex reconnection. In the VFM, reconnections are performed algorithmically by a procedure which reduces the vortex length by a small amount (length being a proxy of energy) to model acoustic energy losses revealed by GPE simulations<sup>35,40</sup>, whereas helicity is unconstrained. Supplementary Material Fig. 4 shows that during an isolated reconnection helicity changes by an amount  $\Delta H$  as (as expected) the relative proportions of local and nonlocal velocity fields and the vortex topology change. These helicity jumps  $\Delta H$  are larger than the numerical fluctuations of helicity during pre - and post - reconnection evolution, but, being either positive or negative, may tend to cancel out, as observed for instance in Fig. 2 (right) when the statistically steady states have been reached. Supplementary Fig. 4 also clearly shows that, as the reconnection cusp relaxes (a feature also observed in experiments<sup>41</sup>), packets of Kelvin waves carry helicity away.

## Discussion

The popular model of the superfluid vortex core, based on the Gross-Pitaevskii equation (GPE), has features (the diverging velocity and the Dirac delta function vorticity localized on the centerline) which complicate the definition of helicity, as debated in the current literature. Although mathematically interesting, for the sake of progress in investigating superfluid turbulence properties, the more physical model of the vortex core<sup>25,26</sup> which we have described should be taken into account.

In this letter, we have proposed a definition of superfluid helicity which uses the most recent information about the structure of the vortex core in <sup>4</sup>He arising from N-body quantum mechanics, accounting for particles' correlations and avoiding the simplifying assumption of the Onsager-Feynman phase. In the more physically realistic model, the core of a quantum vortex is a thin region of depleted but non-vanishing density where the velocity is proportional to the radial distance  $r$ ; near the edge of the core, the density exhibits spatial oscillations corresponding to a standing roton wavepacket; at larger radial distances, the velocity decreases as  $1/r$ , as the GPE vortex. The superfluid vortex core is therefore a small tubular region of constant vorticity surrounded by irrotational flow. Helicity can therefore be defined as in an ordinary (classical) fluid, see Eq. (1).

Unfortunately, unlike classical Euler fluids (in which helicity is a constant of motion), in the case of helium we do not have a simple hydrodynamical equation to give a physical interpretation of the superfluid helicity which we have defined. But the numerical simulations of two different regimes of turbulence which we have presented show that superfluid helicity can be interpreted as a combined measure of the non-local contributions to the total velocity field and the vortex tangle's topology. Superfluid helicity is therefore a useful tool to distinguish the two different limiting regimes<sup>17</sup> which have been observed<sup>42-44</sup> in turbulent helium: the Kolmogorov regime<sup>45</sup>, in which the turbulent tangle of vortex lines is partially polarized, characterized by a relatively high value of total helicity  $H$ , and the Vinen regime in which the vortex lines are essentially at random and  $H \simeq 0$ . The former is observed when helium is stirred at large scales by propellers, or flows rapidly along a wind tunnel, or (at very low temperatures in the absence of normal fluid) when vortex rings are injected at high rate. The latter is seen in the presence of a uniform heat flux, which drives superfluid and normal fluid in opposite directions, or (at low temperatures) when the injection rate of vortex ring is small.

Our result should stimulate further study into any large-scale hydrodynamic effects which result from the microscopic details of the superfluid vortex core. Firstly, it has been suggested<sup>25</sup> that energy in the form of non-thermal rotons may be released during vortex reconnections, affecting the time-scale of the turbulent decay. Secondly, the standing roton wavepacket which surrounds the vortex core may become distorted and lose its axial symmetry if the vortex is bent (all existing studies are two-dimensional or refer to a straight three-dimensional vortex) or another vortex is in the vicinity; this effect may break the axisymmetry of the vortex, thus introducing the concepts of ribbon or internal twist which have been rigorously defined for singular (GPE) vortices only recently<sup>23</sup>.

Finally, we note that these results should also translate to the dilute fermionic superfluids. In these systems, vortices are similarly characterised by a non-zero density in the vortex core, with a transition from solid-body-like to irrotational flow away from the core<sup>47,49,50</sup>. These systems offer a unique opportunity to combine experimental control over the core size and density depletion, with microscopic modelling of the vortices and their reconnections<sup>51</sup>.

## Acknowledgements

C.F.B., N.G.P. and L.G. acknowledge the support of the Engineering and Physical Sciences Research Council (Grant No. EP/R005192/1).

## Methods

In the VFM, the velocity of a vortex line at the point  $\mathbf{s}(\xi, t)$  is<sup>32</sup>

$$\frac{d\mathbf{s}}{dt} = \mathbf{v}(\mathbf{s}, t) + \alpha \mathbf{s}' \times (\mathbf{v}_n(\mathbf{s}, t) - \mathbf{v}(\mathbf{s}, t)) - \alpha' \mathbf{s}' \times [\mathbf{s}' \times (\mathbf{v}_n(\mathbf{s}, t) - \mathbf{v}(\mathbf{s}, t))],$$

where  $\mathbf{v}_n(\mathbf{s}, t)$  is the velocity of the normal fluid at  $\mathbf{s}$ , and  $\alpha$  and  $\alpha'$  are small friction coefficients<sup>46</sup>. The total superfluid velocity at  $\mathbf{s}$  consists of two parts:

$$\mathbf{v}(\mathbf{s}, t) = \mathbf{v}^{near}(\mathbf{s}, t) + \mathbf{v}_{nl}(\mathbf{s}, t),$$

where

$$\mathbf{v}^{near}(\mathbf{s}, t) = \frac{\kappa}{4\pi} \ln\left(\frac{R_c}{a_0}\right) \mathbf{s}' \times \mathbf{s}'',$$

is the (desingularised) contribution arising from the local curvature at  $\mathbf{s}$ , directed in the binormal direction, with  $\mathbf{s}' = \partial\mathbf{s}/\partial\xi$ ,  $\mathbf{s}'' = \partial^2\mathbf{s}/\partial\xi^2$  and  $R_c = 1/|\mathbf{s}''|$  being the local radius of curvature, and

$$\mathbf{v}_{nl}(\mathbf{s}) = \mathbf{v}_{ext}(\mathbf{s}, t) + \frac{\kappa}{4\pi} \oint_{\mathcal{L}'} d\xi' \frac{\mathbf{s}'(\xi', t) \times [\mathbf{s}(\xi, t) - \mathbf{s}(\xi', t)]}{|\mathbf{s}(\xi, t) - \mathbf{s}(\xi', t)|^3},$$

where the Biot-Savart line integral extends over all vortex lines avoiding the line elements near  $\mathbf{s}$ .

The numerical code is based on a variable Lagrangian discretization along the vortex lines<sup>32</sup> such that the minimum separation between discretization points is held at  $\Delta\xi/2 = 7.5 \times 10^{-3}$  cm. Integration in time is achieved using a third order Runge-Kutta scheme with a timestep  $\Delta t = 4 \times 10^{-3}$  s. Vortex reconnections are implemented algorithmically<sup>32,38</sup>. All simulations are performed in a cubic domain of size  $D = 1$  cm at temperature  $T = 1.9$  K (typical of experiments) corresponding to  $\alpha = 0.206$  and  $\alpha' = 0.009$ .

The initial condition for the superfluid vortex tangle consists of a number of randomly oriented loops of different radius. The evolution is computed until a statistical steady-state regime is achieved, characterized by vortex line density fluctuating around an average value  $L = 100 \text{ cm}^{-2}$ . In the first set of simulations we model thermal counterflow at small heat flux, setting  $\mathbf{v}_n = 0.08$  cm/s and  $\mathbf{v}_{ext} = 0$  (in other words, we are in the reference frame of the external superflow which moves towards the heater). In the second set of simulations, we use the steady ABC flow<sup>39</sup>

$$\mathbf{v}_n(\mathbf{r}) = (A \sin(kz) + C \cos(ky), (B \sin(kx) + A \cos(kz), (C \sin(ky) + B \cos(kx)),$$

to model coherent structures present in the turbulent normal fluid, with  $A = B = C = 0.03$  cm/s and  $k = 2\pi \text{ cm}^{-1}$

## References

1. Kleckner, D., & Irvine, W.T.M. Creation and dynamics of knotted vortices. *Nature Phys.* **9**, 253 (2013).
2. Moffatt, H.K. Degree of knottedness of tangled vortex line, *J. Fluid Mech.* **35**, 117 (1969).
3. Moffatt, H.K., & Ricca, R.L. Helicity and the Călugăreanu invariant. *Proc. Roy. Soc. London A* **439**, 411 (1992).
4. Kraichnan, R.H. Helical turbulence and absolute equilibrium, *J. Fluid Mech.* **59**, 745 (1973).
5. Biferale, L., Musacchio, S. & Toschi, F. Inverse energy cascade in three-dimensional isotropic turbulence, *Phys. Rev. Lett.* **108**, 164501 (2012).
6. Brandenburg, A. & Subramanian K., Astrophysical magnetic fields and nonlinear dynamo theory, *Phys. Reports* **417**, 1 (2005).
7. Kleckner, D., Kauffman, L.H., & Irvine, W.T.M. How superfluid vortex knots untie. *Nature Phys.* **12**, 650 (2015).
8. X. Liu, X. & Ricca, R.L. Knots cascade detected by a monotonically decreasing sequence of values. *Sci. Rep.* **6**, 24118 (2016).
9. Scheeler, M.W., van Rees, W.M., Kedia, H., Kleckner, D., & Irvine, W.T.M. Complete measurement of helicity and its dynamics in vortex tubes, *Science* **357**, 487 (2017).
10. Barenghi, C.F. & Parker, N.G. *A Primer on Quantum Fluids* (Springer 2016).
11. Skrbek, L., & Sreenivasan, K.R. Developed superfluid turbulence and its decay. *Phys. Fluids* **24**, 011301 (2012).
12. Barenghi, C.F., Skrbek, L. & Sreenivasan, K.R. Introduction to quantum turbulence. *Proc. Nat. Acad. Sci. USA*, **111**, (Suppl. 1), 4647 (2014).
13. Marakov, A., Gao, J., Van Sciver, S.W., Ihas, G.G., McKinsey, D.N. & Vinen, W.F. Visualization of the normal-fluid turbulence in counterflowing superflowing  $^4\text{He}$ . *Phys. Rev. B* **91**, 094503 (2015).
14. Baggaley, A.W. Tsepelin, V., Barenghi, C.F., Fisher, S.N., Pickett, G.R., Sergeev, Y.A., & Suramlshvili, N. Visualizing pure quantum turbulence in superfluid  $^3\text{He}$ : Andreev reflection and its spectral properties. *Phys. Rev. Lett.* **115**, 015302 (2015).
15. Barenghi, C.F., L'vov, V., & Roche, P.E. Experimental, numerical and analytical velocity spectra in turbulent quantum fluid. *Proc. Nat. Acad. Sci. USA*, **111**, (Suppl. 1) 4683 (2014).
16. Baggaley, A.W., Laurie, J., & Barenghi, C.F. Vortex-density fluctuations, energy spectra, and vortical regions in superfluid turbulence. *Phys. Rev. Lett.* **109**, 205304 (2012)
17. Barenghi, C.F., Sergeev, Y.A., & Baggaley, A.W. Regimes of turbulence without an energy cascade. *Sci. Reports* **6**, 35701 (2016).
18. Bewley G.P., Paoletti M.S., Sreenivasan K.R. & Lathrop D.P. Characterization of reconnecting vortices in superfluid helium. *Proc. Nat. Acad. Sci. USA* **105**. 13707 (2008).
19. Serafini, S., Galantucci, L., Iseni, E., Bienaimé, T., Bisset, R.N., Barenghi, C.F., Dalfovo, F., Lamporesi G. & Ferrari, G. Vortex reconnections and rebounds in trapped atomic Bose–Einstein condensates. *Phys. Rev. X* **7**, 021031 (2017).
20. Hänninen, R., Hietala, N., & Salman, H. Helicity within the vortex filament model. *Sci. Rep.* **6**, 37571 (2016).
21. diLeoni, P.C., Mininni, P., & Brachet, M.E. Dual cascade and dissipation mechanisms in helical quantum turbulence. *Phys. Rev. A* **95**, 053636 (2017).
22. Zuccher, S., & Ricca, R.L. Twist effects in quantum vortices and phase defects. *Fluid Dyn. Res.* **50**, 011414 (2018).
23. Salman, H. Helicity conservation and twisted Seifert surfaces for superfluid vortices. *Proc. Roy. Soc. A* **473**, 20160853 (2018).
24. Donnelly, R.J., Donnelly, J.A., & Hills, R.N. Specific heat and dispersion curve for helium II. *J. Low Temp. Phys.* **44**, 471 (1981).
25. Amelio, I., Galli, D.E., & Reatto, L. Probing quantum turbulence in  $^4\text{He}$  by quantum evaporation measurements. *arXiv:1802.07071* (2018).
26. Galli, D.E., Reatto, L., & Rossi, M. Quantum Monte Carlo study of a vortex in superfluid  $^4\text{He}$  and search for a vortex state in the solid. *Phys. Rev. B* **89**, 224516 (2014).
27. Berloff, N.G., & Roberts, P.H. Motions in a bose condensate: VI. Vortices in a nonlocal model. *J. Phys. A. Math Gen.* **32**, 5611 (1999).

28. Ortiz, G. & Ceperley, D.M. Core structure of a vortex in superfluid  $^4\text{He}$ . *Phys. Rev. Lett.* **75**, 4642 (1995).
29. Sadd, M., Chester, G.V., & Reatto, L. Structure of a vortex in superfluid  $^4\text{He}$ . *Phys. Rev. Lett.* **79**, 2490 (1997).
30. Sherwin-Robson, L.K., Barenghi, C.F., & Baggaley, A.W., Local and nonlocal dynamics in superfluid turbulence. *Phys. Rev. B* **91**, 104517 (2015).
31. G.W. Rayfield & F. Reif. Quantized vortex rings in superfluid helium. *Phys. Rev.* **136** A 1194 (1964).
32. Schwarz, K.W. Three-dimensional vortex dynamics in superfluid  $^4\text{He}$ : homogeneous superfluid turbulence. *Phys. Rev. B* **38**, 2398 (1988).
33. S. Yui, M. Tsubota & H. Kobayashi. Three-dimensional coupled dynamics of the two-fluid model in superfluid  $^4\text{He}$ : deformed velocity profile of normal fluid in thermal counterflow. *Phys. Rev. Lett.* **120**, 155301 (2018).
34. Koplik, J. & Levine, H. Vortex reconnections in superfluid helium. *Phys. Rev. Letters* **71**, (1993).
35. Zuccher, S., Caliarì, M., Baggaley, A.W. & Barenghi, C.F. Quantum vortex reconnections. *Phys. Fluids* **24**, 125108 (2012).
36. Rorai, C., Skipper J., Kerr, R, M., Sreenivasan, K. R. Approach and separation of quantised vortices with balanced cores. *J. Fluid Mech.* **808**, 641 (2016)
37. Vilhois, A., Proment, D., Krstulovic, G. Universal and nonuniversal aspects of vortex reconnections in superfluids. *Phys. Rev. Fluids* **2**, 044701 (2017)
38. Baggaley, A.W. The sensitivity of the vortex filament method to different reconnection models. *J. Low Temp. Phys.* **168**, 18 (2012).
39. Barenghi, C.F., Bauer, G.G., Samuels, D.C., & Donnelly, R.J. Superfluid vortex lines in a model of turbulence. *Phys. Fluids* **9**, 2631 (1997).
40. Leadbeater, M., Winiiecki, T., Samuels, D.C., Barenghi, C.F., & Adams, C.S. Sound emission due to superfluid vortex reconnections, *Phys. Rev. Lett.* **86** 1410 (2001).
41. Fonda, E., Meichle, D.P., Ouettette, N.T., Hormoz, S., & Lathrop, D.P. Direct observation of Kelvin waves excited by quantized vortex reconnections. *Proc. Nat. Acad. Sci. USA* **111**, (Suppl. 1) 4707 (2014).
42. Volovik, G.E., Classical and quantum regimes of superfluid turbulence. *JETP Lett.* **78**, 533 (2003).
43. Walmsley, P.M., & Golov, A.I. Quantum and quasiclassical types of superfluid turbulence. *Phys. Rev. Lett.* **100**, 245301 (2008).
44. Bradley, D.I., Clubb, D.O., Fisher, S.N., Guénault, A.M., Haley, R.P., Matthews, J.C., Pickett, G.R., Tsepelin, V., & Zaki, K. Decay of pure quantum turbulence in superfluid  $^3\text{He}$ -B. *Phys. Rev. Lett.* **96**, 035301 (2006).
45. Salort, J., Baudet, C., Castaing, B., Chabaud, B., Davidaud, F., Didelot, T., Diribarne, P., Dubrulle, B., Cagne, Y., Gauthier, F., Girard, A., Hébral, B., Rousset, B. Thibault, P. & Roche, P-E. Turbulent velocity spectra in superfluid flows. *Phys. Fluids* **22**, 125102 (2010).
46. Donnelly, R.J., & Barenghi, C.F. The observed properties of liquid helium at the saturated vapor pressure. *J. Phys. Chem. Ref. Data* **27**, 1217 (1998).
47. Nygaard, N., Bruun, G. M., Clark, C. W. & Feder, D. L. Microscopic Structure of a Vortex Line in a Dilute Superfluid Fermi Gas. *Phys. Rev. Lett.* **90**, 210402 (2003).
48. Bulgac, A. & Yu, Y. Vortex State in a Strongly Coupled Dilute Atomic Fermionic Superfluid. *Phys. Rev. Lett.* **91**, 190404 (2003).
49. Bulgac, A. & Yu, Y. Vortex State in a Strongly Coupled Dilute Atomic Fermionic Superfluid. *Phys. Rev. Lett.* **91**, 190404 (2003).
50. Sensarma, R., Randeria, M. & Ho, T-L. Vortices in Superfluid Fermi Gases through the BEC to BCS Crossover. *Phys. Rev. Lett.* **96**, 090403 (2006).
51. Bulgac, A., Luo, Y-L., Magierski, P., Roche, K. J. & Yu, Y. Real-Time Dynamics of Quantized Vortices in a Unitary Fermi Superfluid. *Science* **332**, 1288 (2011).

## Supplementary Material

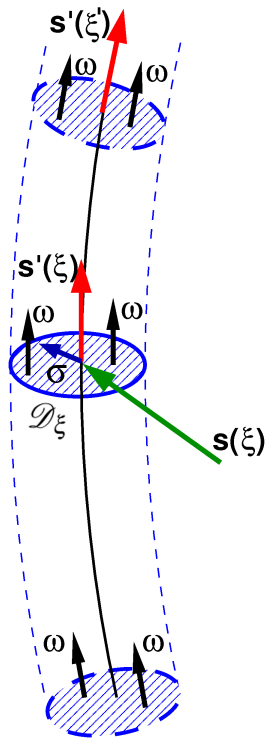


**Figure 3.** Schematic diagram of the vortex line near the point  $\mathbf{s}(\xi)$ . The centerline is the solid curve with the red arrows indicating the unit tangent vector  $\mathbf{s}'(\xi)$  where  $\xi$  is arc length. The dashed blue curve shows the vortex tube of radius  $a_0$  centered on the vortex line; the dashed blue discs  $\mathcal{D}_\xi$  are cross-sections of the tube; within the vortex tube, the vorticity  $\boldsymbol{\omega}$  is constant. The position vector  $\boldsymbol{\sigma}$  on the disc  $\mathcal{D}_\xi$  is indicated in blue.

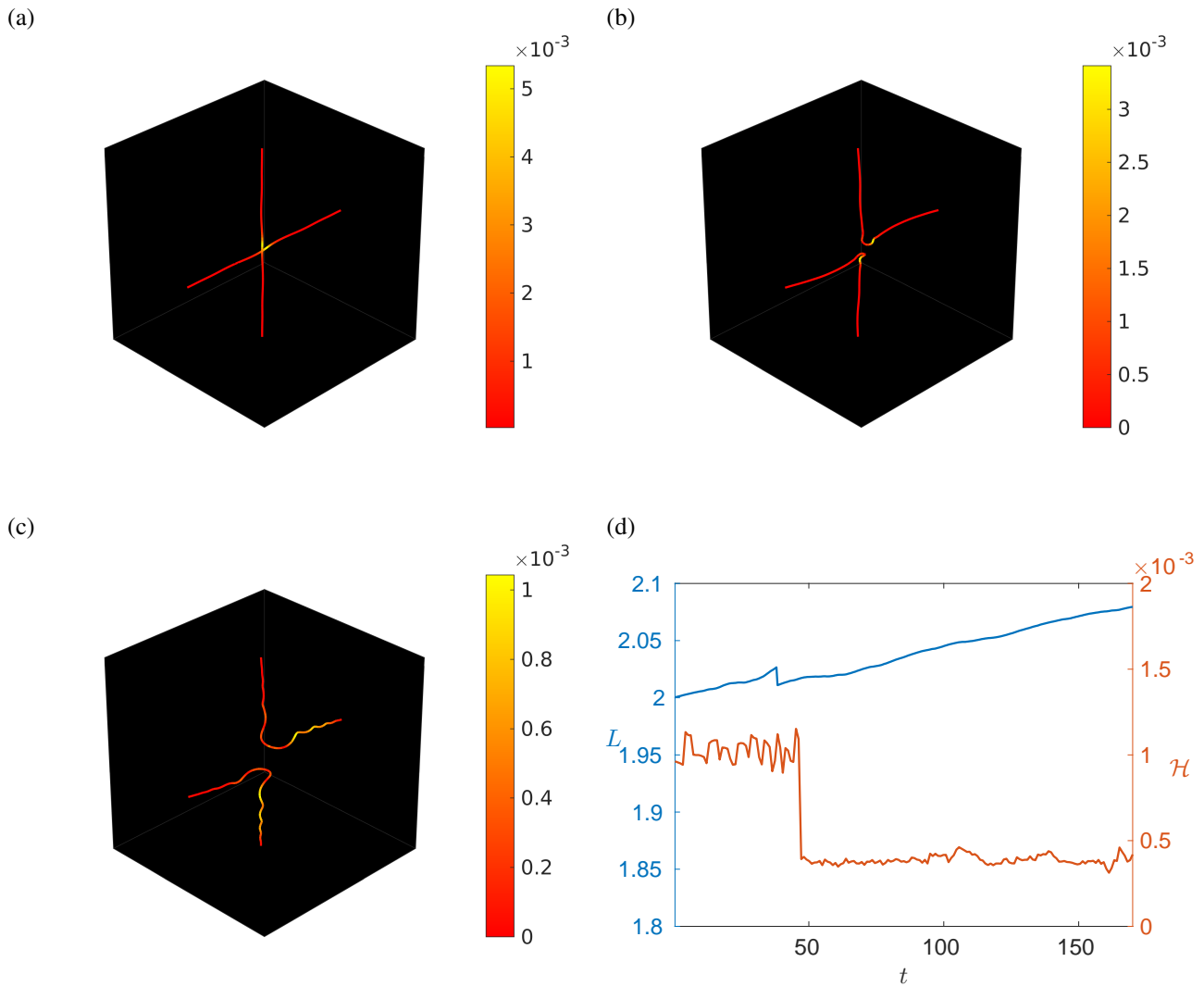


**Figure 4.** (a)-(c) Snapshots of two initially orthogonal vortices undergoing a reconnection at  $T = 0$  (hence the friction coefficients are set to  $\alpha = \alpha' = 0$ ). The calculation is performed using the VFM in a periodic domain. The vortex lines are colour-coded according to the local absolute helicity density. Regions with low helicity density are red, regions with high helicity density are yellow. In (c), note the Kelvin wavepacket which carries helicity away from the relaxing reconnection cusp. (d) Time series showing the evolution of the vortex line density,  $L$  (in blue), and of the volume integrated helicity,  $H$  (in red); the reconnection occurs at  $t \approx 48$  s. The reconnection algorithm does not constrain  $H$  (which jumps at the reconnection by an amount larger than the typical numerical fluctuations) and decreases  $L$  to model acoustic energy losses. During pre- and post-reconnection evolutions, energy and helicity are conserved (because there is no friction) while the vortex length is slightly stretched.